Effect of Soft Viscoelastic Biopolymer on the Undrained Shear Behavior of Loose Sands

Dong-Hwa Noh[1]; Wonjun Cha[2]; J. Carlos Santamarina, A.M.ASCE[3]; Gye-Chun Cho[4]; and Tae-Hyuk Kwon, A.M.ASCE[5]

Abstract: Soft viscoelastic biological products such as biopolymers and biofilms have recently garnered significant interest as alternative biogrout materials for ground improvement because of their nontoxic and biodegradable characteristics. However, the impact of soft gel-like viscoelastic pore fillers on the undrained response of treated soils remains poorly understood. This study involves undrained triaxial compression tests with concurrent shear wave velocity measurements of loose contractive sands treated with soft gelatin. The specimens experience two distinct loading-gelation sequences, either consolidation before gelation (CbG) or confinement after gelation (CaG). Results reveal that the shear wave velocity can be used as an indicator of the effective stress carried by the granular skeleton. The inclusion of the viscoelastic biopolymer hinders the contractive tendency, diminishes postpeak softening, and increases the undrained shear strength of loose contractive sands. These effects become more pronounced for stiffer biopolymers because they provide an enhanced skeletal support against chain buckling and contraction. The presence of biopolymers increases the normalized undrained shear strength from $S_u/\sigma_o' = \sim 0.1$ to ~ 1.4, particularly at low effective confining stress. The biopolymers alter the terminal state in the p'-q-e space. Therefore, critical states should be reconsidered for biopolymer-treated sands. The confinement-gelation sequence affects the effective stress supported by the granular frame and thus has pronounced effects on the undrained shear strength. This suggests the potential use of viscoelastic pore fillers as an effective treatment of loose sands prone to liquefaction. **DOI: 10.1061/(ASCE)GT.1943-5606.0002582.**

Author keywords: Biopolymer; Gelatin; Viscoelastic inclusion; Undrained load–deformation behavior; Undrained shear strength; Contractive failure; Loose sand; Loading history; Critical state.

Introduction

Grout injection is used to improve loose contractive sands that are prone to liquefaction. Injected chemical grouts bind soil grains, increase the undrained shear strength, and thus reduce the liquefaction potential of soils (Gallagher and Mitchell 2002; Xanthakos 1994; Karol 2003). Typical materials include cement, gypsum, sodium silicate, acrylates, acrylamides, and polyurethanes. Various efforts have characterized and modeled the mechanical behavior of soils cemented with brittle chemical grout materials (e.g., Clough et al. 1981; Airey and Fahey 1991; Lade and Overton 1989; Fernandez and Santamarina 2001; Wang and Leung 2008). However, the injection of chemical grouts is often problematic due to water pollution and environmental regulations (DeJong et al. 2010). With societal demands for environmentally friendly construction materials and techniques, the use of gel-like biopolymers has recently garnered significant interest as an alternative to chemical grout materials for ground improvement because of their nontoxic and biodegradable characteristics (Ivanov and Chu 2008; DeJong et al. 2010; Cabalar et al. 2017; Im et al. 2017). Furthermore, biopolymers are known to improve erosion resistance, increase water retention, and promote vegetation (Kwon et al. 2017, 2019; Cho and Chang 2018; Ham et al. 2018; Tran et al. 2019; Kim et al. 2019). In contrast to brittle cemented soils, the impact of soft viscoelastic inclusions, such as gel-like biopolymers, on the mechanical response of treated soils remains poorly understood.

The sudden contractive failure of saturated sands results from positive excess pore pressure generated during undrained loading (Terzaghi et al. 1967; Castro 1969; Casagrande 1976; Yamamuro and Lade 1997; Santamarina et al. 2019). This excess pore pressure reduces the effective stress and hence the undrained shear strength of sands, and in some extreme cases may lead to flow liquefaction (Robertson and Wride 1998; Yoshimine et al. 1999). The inclusion of viscous biopolymers, such as guar gum, gellan gum, beta-glucan, and xanthan gum, has been proven to effectively increase soil strength, although the extent of improvement differs with the host soil's baseline strength, curing time, water content, and biopolymer characteristics (e.g., Chang and Cho 2012; Chen et al. 2013; Latifi et al. 2016; Muguda et al. 2017; Soldo et al. 2020). Earlier studies used uniaxial compression (UC), unconsolidated-undrained loading (UU), vane shear, fall cone,

[1]Postdoctoral Fellow, Dept. of Civil and Environmental Engineering, Korea Advanced Institute of Science and Technology, Deajeon 34141, South Korea. Email: dhnoh@kaist.ac.kr

[2]Ph.D. Candidate, Dept. of Earth Science and Engineering, King Abdullah Univ. of Science and Technology, Thuwal 23955, Saudi Arabia. ORCID: https://orcid.org/0000-0002-3897-2863. Email: wonjun.cha@kaust.edu.sa

[3]Professor, Dept. of Earth Science and Engineering, King Abdullah Univ. of Science and Technology, Thuwal 23955, Saudi Arabia. Email: carlos.santamarina@kaust.edu.sa

[4]Professor, Dept. of Civil and Environmental Engineering, Korea Advanced Institute of Science and Technology, Deajeon 34141, South Korea. Email: gyechun@kaist.ac.kr

[5]Associate Professor, Dept. of Civil and Environmental Engineering, Korea Advanced Institute of Science and Technology, Deajeon 34141, South Korea (corresponding author). ORCID: https://orcid.org/0000-0002-1610-8281. Email: t.kwon@kaist.ac.kr

Note. This manuscript was submitted on February 25, 2020; approved on April 5, 2021; published online on June 3, 2021. Discussion period open until November 3, 2021; separate discussions must be submitted for individual papers. This paper is part of the ***Journal of Geotechnical and Geoenvironmental Engineering***, © ASCE, ISSN 1090-0241.

and direct shear tests, and had limited control on the confining stress or fluid saturation. In fact, the undrained load–deformation response of biopolymer-treated sands under triaxial stress conditions is scarcely examined.

This study explores the load–deformation behavior of loose contractive sands treated with soft viscoelastic biopolymers when subjected to undrained loading. The analysis emphasizes the extent to which soft viscoelastic pore fillers alter the contractive behavior and improve the undrained shear strength. Gelatin was chosen as a model biopolymer to represent the soft viscoelastic medium. The confinement and gelation history may affect the mechanical behavior of the gelatin-treated sands in a way similar to that of cemented sands (Clough et al. 1981; Consoli et al. 2010; Khan et al. 2006; Yun and Santamarina 2005; Dai and Santamarina 2017). For example, the failure of cementing bonds governs the overall strength of a cemented sand when the cementing process precedes the confinement. On the other hand, when the confinement precedes the cementing process, both the baseline strength of the granular frame and the strength of the cementing agent contribute to the cemented sand strength.

These contrasting results call for the examination of two extreme confinement-gelation sequences: consolidation *before* gelation (CbG), and confinement *after* gelation (CaG). We use triaxial compression tests to identify the effect of gelatin treatment and formation sequence on the stress–strain responses of loose and contractive sands during undrained loading while simultaneously monitoring changes in shear wave velocity. Results provide a unique experimental data set and new insights into the feasibility of soft viscoelastic biopolymers to improve the undrained strength of loose contractive sands that are prone to liquefaction.

Materials and Methods

Gelatin as a Model Biopolymer

Gelatin was chosen as a model biopolymer to represent soft viscoelastic inclusions. It is a translucent, colorless, nearly tasteless solid substance derived from the collagen in animal skins and bones. Gelatin is an irreversibly hydrolyzed form of collagen. It consists of various amino acids, predominantly composed of glycine, proline, hydroxyproline, glutamic acid, arginine, and alanine, and its chemical formula is typically expressed as $C_{102}H_{151}O_{39}N_{31}$ (Bogue 1923; Imeson 2010). The gelatin used in this study was Type B extracted from bovine hide (Davis Food Ingredients, Auckland, New Zealand).

Gelatin is a viscoelastic material and shows a wide range of physical properties, which vary with the gelatin-water mixing ratio and curing conditions, such as temperature, humidity, and curing time (Imeson 2010; Gómez-Estaca et al. 2011). Gelatin has thermoreversible characteristics due to hydrogen and van der Waals bonds. The sol-gel transition is reversed by heating and cooling, and can be repeated several times without loss of gel characteristics (Imeson 2010; Kavanagh et al. 2013).

Curing and gelation took place in this study over 24 h at an ambient temperature of 20°C. We mixed 8.7, 13.64, 19.05, and 25 g gelatin with 100 g deionized water to prepare four gelatin concentrations: $C = 8\%$, 12%, 16%, and 20% (Table S1). The mixing temperature was 60°C to ensure the complete dissolution of gelatin. Gelation binds gelatin and water molecules (Bohidar and Jena 1993); all available water was bound to gelatin in this study, and hence there was no free water left on the cured gelatin surface.

The mechanical properties of pure gelatin samples were measured for the different gelatin concentrations and included uniaxial compressive strength and both small- and large-strain elastic moduli (Figs. S1–S3). The measured uniaxial compressive strength ranged from $q_u = 2.87$ to 15.17 kPa and the Young's modulus ranged from $E = 4.5$ to 32.4 kPa, as a function of gelatin concentration (Fig. S1). Rod and shear wave velocity values ranged from $V_L = 1.4$ to 6.3 m/s and from $V_S = 0.5$ to 2.6 m/s (Fig. S3).

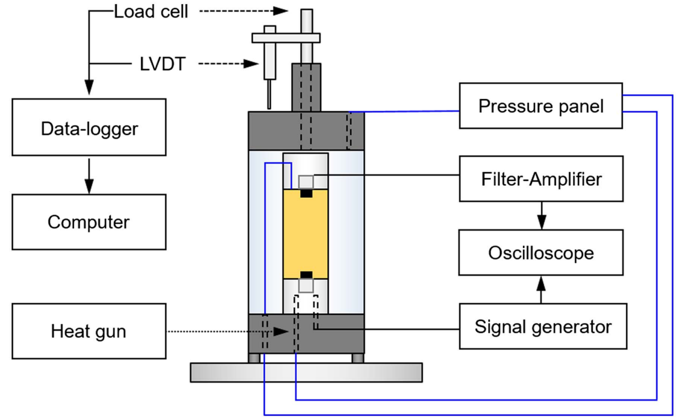

Fig. 1. Instrumented triaxial cell and peripheral electronics.

Test Equipment

Fig. 1 presents the instrumented triaxial cell used in this study. The axial compression load was imposed at a constant displacement rate. The pressure panel controlled both the cell and fluid pressures. The instrumentation included a load cell to measure the vertical load and a linear variable differential transformer to monitor the vertical displacement. A pair of bender elements was installed on the top and bottom caps to capture shear wave signals during deviator loading; the input signal was a square wave with a 20-Hz repetition rate and an amplitude of 10 V (function generator: Keysight, Model 33210A, Santa Rosa, California). An oscilloscope (Keysight, Model DSOX3024A) stored the signals received by the top bender element after preconditioning by a filter amplifier (Krohn-Hite, Model 3384, Brockton, Massachusetts, bandpass filter from 500 to 200 kHz).

Specimen Preparation

The experiments used clean coarse silica sand (KAUST 20/30, BMS, Jeddah, Saudi Arabia) with the following index properties: specific gravity $G_s = 2.65$, mean grain size $D_{50} = 0.72$ mm, maximum void ratio $e_{\max} = 0.786$, and minimum void ratio $e_{\min} = 0.533$.

The reference tests used gelatin-free sand specimens. The target relative density was controlled to be less than $D_r < 50\%$ to promote a contractive response and greater than $D_r > 50\%$ to ensure dilative behavior. Dry sand was first air-pluviated into a membrane stretched over a split mold. All specimens were prepared by air pluviation and had a diameter of 50 mm and a target height of 100 mm. After applying a vacuum of ~20 kPa to the dry sand specimen, the split mold was removed, the pressure cell was assembled, and the confining stress ~30 kPa was applied. Deaired and deionized water was introduced into the specimen for water saturation with a pressure difference of 3 kPa, followed by a 200- to 300-kPa backpressure at a constant effective stress of 30 kPa. At the end of saturation, the B-value was greater than 0.94 in all tests. Thereafter, sand specimens were subjected to the effective confining stress of $\sigma'_o = 100$ kPa or $\sigma'_o = 400$ kPa by simultaneously controlling the cell and back pressures. Specimens were kept for

J. Geotech. Geoenviron. Eng., 2021, 147(8): 04021072

Table 1. Experiment conditions

Loading history	Initial confining stress, σ_o (kPa)	Gelatin concentration, c (%)	Initial void ratio, e	Final void ratio, e	Relative density, D_r (%)	Undrained shear strength, S_u (kPa)
CbG	100	8	0.716	0.663	49	108
		12	0.726	0.661	49	122
		16	0.734	0.673	45	127
		20	0.735	0.673	45	144
	400	8	0.742	0.673	44	149
		12	0.767	0.685	40	201
		16	0.736	0.671	45	261
		20	0.737	0.682	41	269
CaG	50	8	0.680	0.680	42	16
		12	0.693	0.693	37	22
		16	0.667	0.667	47	89
		20	0.699	0.699	34	67
	100	8	0.685	0.685	40	15
		12	0.704	0.704	32	27
		16	0.692	0.692	37	48
		20	0.667	0.667	47	78
Biopolymer-free sand	100	0	0.690	0.679	42	15
		0	0.663	0.652	53	255
	400	0	0.722	0.684	40	38
		0	0.742	0.673	45	55
		0	0.672	0.632	61	395

more than 1 h until volume change ceased. The final relative density of the biopolymer-free specimens ranged from $D_r = 31\%$ to 61% after isotropic effective confinement.

Preparation of the biopolymer-treated sand specimens started by pouring a warm gelatin solution of 60°C into the stretched membrane. The dry sand was then wet-pluviated into this solution to ensure homogeneous mixing and full saturation of the specimens. The final relative density of these biopolymer-treated specimens ranged from $D_r = 32\%$ to 48% after isotropic confinement.

Deviator Loading: Two Loading Histories

Consolidation before Gelation

The loosely packed sand specimens saturated with the warm gelatin solution were subjected to a cell pressure of ~40 kPa while hot water at ~75°C circulated through the triaxial cell to completely melt the gelatin contained within the specimens. We also heated an external flow line to avoid gelation (Fig. 1). The confining stress was then elevated to the target initial confining effective stresses of either $\sigma'_o = 100$ kPa or $\sigma'_o = 400$ kPa under drained conditions for 30 min. The drained gelatin volume allowed calculations of specimen volume changes during consolidation. Following the consolidation phase, the gelatin-treated sand specimens were cured for 24 h at ~20°C while maintaining a constant cell pressure. Through additional batch experiments, we confirmed that the gelatin volume did not measurably change during the cooling from 75°C to 20°C.

Confinement after Gelation

The sand specimens saturated with warm gelatin solutions were cured for 24 h at ~20°C without confining stress. After complete gelation, the cell pressure was elevated to the initial confining stress of either $\sigma_o = 50$ kPa or $\sigma_o = 100$ kPa. The pore pressure valve remained open for a consolidation time of approximately 30 min; however, there was no measurable volume change in the specimen.

Shearing by Deviator Loading

The pore pressure valve was closed to enforce undrained deviator loading for both CbG and CaG specimens. The vertical deformation rate was kept constant at 1 mm/min, equivalent to a vertical strain rate of 1%/min. Shearing continued to a vertical strain greater than 20%. Gelatin plugged pores and flow lines once the gelatin hardened; therefore, pore fluid pressure measurements were not possible during the undrained deviator loading of the biopolymer-treated sands. Shear wave signatures were acquired every minute during deviator loading (see Figs. S4–S6 for shear wave signatures).

Results and Analyses

Table 1 details the test conditions and key results for all tests. CbG and CaG cases tested at 100 kPa confining stress allow for direct comparisons between the two load-gelation histories [Figs. 2(a) and 3(b)].

Stress–Strain Response

Figs. 2 and 3 show the measured deviator stress–strain responses obtained from specimens prepared with five different gelatin concentrations and the two extreme load-gelation histories, CbG and CaG. The stress–strain responses of biopolymer-free, water-saturated sands are superimposed on these figures for comparison. The deviator stress is defined as $q = (\sigma_1 - \sigma_3)/2 = \sigma_d/2$, where σ_1 is the major principal stress, σ_3 is the minor principal stress, and σ_d is the deviator vertical stress applied by the piston.

Consolidation before Gelation

The biopolymer-free $C = 0\%$, loosely packed water-saturated sand specimens exhibit a contractive postpeak softening response due to the positive excess pore pressure generated during undrained shearing [Figs. 2(a and b); the biopolymer-free specimen at $D_r = 53\%$ shows dilative behavior under $\sigma'_o = 100$ kPa]. Furthermore, the contractive tendency increases as the mean effective stress increases (Schofield and Wroth 1968; Wood 1990). Eventually, the biopolymer-free specimen packed at $D_r = 61\%$ shows a dilative response and negative excess pore pressure under $\sigma_o' = 400$ kPa.

The biopolymer-treated sands do not exhibit postpeak softening, but a rather complex load–deformation behavior (Fig. 2). The deviator stress initially increases in a way similar to the biopolymer-free sands. Then there is a minor decrease in deviator resistance as particles attempt to rearrange. However, soon thereafter, the stress–strain trends show a rapid increase in the deviator stress and reach a large-strain strength that increases with the gelatin concentration C [Figs. 2(a and b)]. Clearly, the presence of the soft biopolymer in pores prevents the internal structural collapse of loose sands and increases the undrained shear strength.

Confinement after Gelation

Fig. 3 shows the stress–strain responses of the biopolymer-treated specimens that were confined after gelation. Stress–strain curves reveal mostly strain-hardening behavior, in contrast to the biopolymer-free specimens. The applied confining stress has a minimal impact on the undrained shear strength [e.g., $\sigma_o = 50$ kPa in Fig. 3(a) and $\sigma_o = 100$ kPa in Fig. 3(b)], yet the strength increases with gelatin concentration. This suggests that the confining stress applied after gelation is not felt by the granular skeleton.

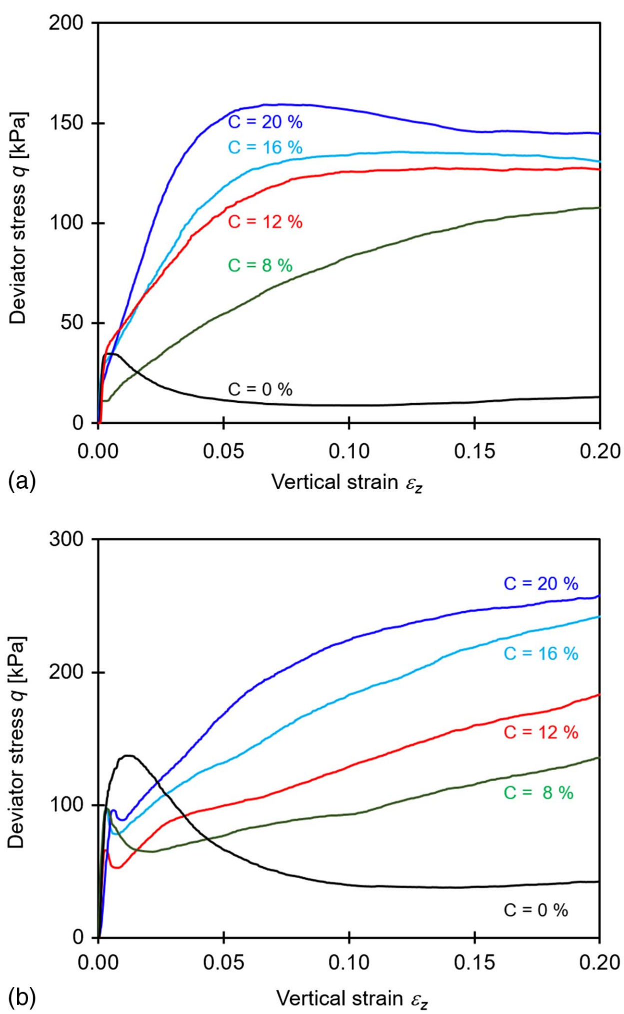

Fig. 2. Sand with biopolymer CbG and biopolymer-free sand. Response during undrained deviator loading for an initial isotropic effective confinement: (a) $\sigma_o' = 100$ kPa; and (b) $\sigma_o' = 400$ kPa.

Shear Wave Velocity Evolution with Vertical Strain

Biopolymer-Free Sands ($C = 0$)

The effective stress determines the shear stiffness of the granular frame. Therefore, the shear wave velocity V_S can be an indicator of the changes in the mean effective stress (Hardin and Drnevich 1972; Knox et al. 1982; Fam and Santamarina 1995; Aloufi and Santamarina 1995; Cha et al. 2014). Trends in Fig. 4 show a high correlation between the excess pore water pressure and shear wave velocity evolution during undrained axial compression loading. Clearly, the excess pore pressure changes the effective stresses and affects the shear wave velocity in both contractive specimens and dilative specimens.

Consolidation before Gelation

Fig. 5 plots the measured shear wave velocity V_S at both $\sigma_o' = 100$ kPa and $\sigma_o' = 400$ kPa. The initial values are similar to the biopolymer-free specimens: $V_S = \sim 310$ m/s at $\sigma_o' = 100$ kPa and $V_S = \sim 420$ m/s at $\sigma_o' = 400$ kPa. This confirms that the shear wave velocity depends on the effective confining stress and that the gelatin has no effect on the initial shear stiffness. The shear wave velocity of the biopolymer-free specimens decreases with vertical strain due to the generation of positive excess pore pressure. During deviator loading, the shear wave velocity of the biopolymer-treated specimens increases to $V_S = 450$ m/s at $\sigma_o' = 100$ kPa (Fig. 5).

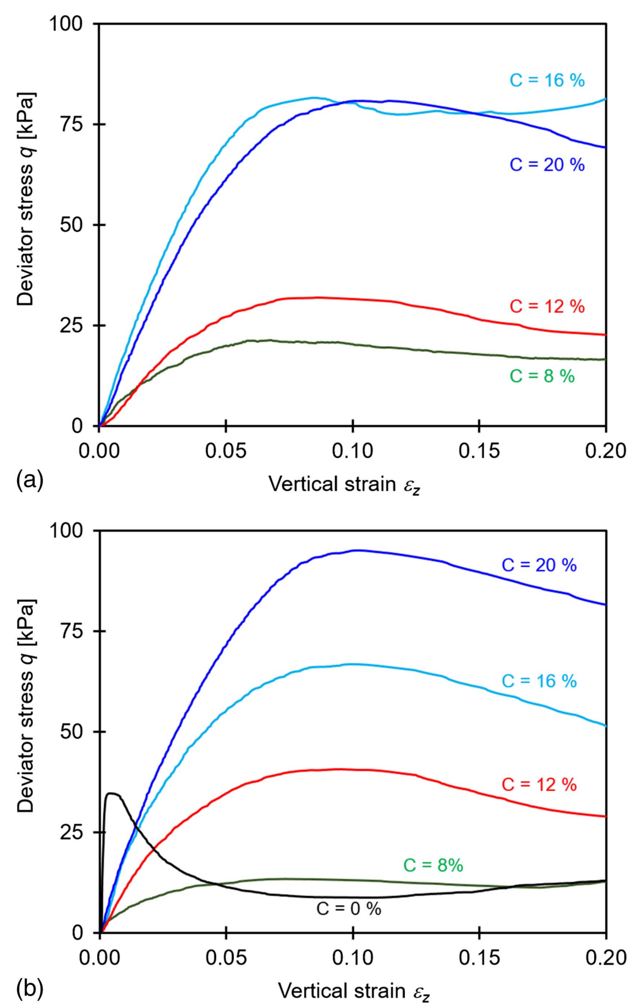

Fig. 3. Sand with CaG biopolymer. Stress–strain response for initial isotropic confinement: (a) $\sigma_o = 50$ kPa; and (b) $\sigma_o = 100$ kPa.

The sand exhibits a more contractive tendency at higher confining stress σ_o'; therefore, biopolymer-treated specimens confined to $\sigma_o' = 400$ kPa show an initial slight decrease in the shear wave velocity. Overall, changes in the shear wave velocity are consistent with the stress–strain response of biopolymer-treated sands, which do not display postpeak softening. At large strains, velocities converge to $V_S = \sim 450$ m/s regardless of the gelatin concentration or the initial effective stress σ_o'.

Confinement after Gelation

Fig. 6 presents the measured shear wave velocities for CaG specimens at both $\sigma_o = 50$ kPa and $\sigma_o = 100$ kPa. Initial velocities after confinement show no consistent confinement effects and range from $V_S = \sim 80$ to 190 m/s at $\sigma_o = 50$ kPa and $V_S = \sim 110$ to 130 m/s at $\sigma_o = 100$ kPa. These values are much lower than in CbG specimens and biopolymer-free specimens (e.g., ~310 m/s in Figs. 4 and 5). This suggests that only a minor part of the confining stress is felt by the granular frame. During undrained deviator loading under both $\sigma_o = 50$ and 100 kPa, the shear wave velocity increases up to a vertical strain of $\varepsilon_z = 0.05$–0.07 and thereafter stays constant or slightly decreases, indicating the gradual engagement of the granular skeleton during shear. Overall, the shear wave velocity–strain curves in Fig. 6 are similar to the stress–strain curves in Fig. 3, and there is a clear effect of the gelatin concentration on the shear wave velocities attained during deviator loading.

Discussion

Undrained Shear Strength

The undrained shear strength S_u is the deviator stress q at large strains herein determined at a vertical strain of $\varepsilon_z \approx 20\%$ [ASTM D4767 (ASTM 2011); Thevanayagam 1998]. Fig. 7 shows the measured undrained shear strength plotted versus gelatin concentration for the various initial confining stresses and loading histories. The undrained shear strength S_u increases with gelatin concentration in both the CbG and CaG cases. These results suggest that biopolymers with higher stiffness and strength provide greater support to the granular frame and prevent the buckling of chains [Figs. 7(a) and S1]. Previous studies using soils treated with beta-glucan and xanthan biopolymers show similar trends [unconfined compression: Chang and Cho (2012), Chen et al. (2013), Latifi et al. (2016), and Soldo et al. (2020); vane shear: Cho and Chang (2018)].

Fig. 7(b) depicts the undrained shear strength normalized by the initial confining stress. Results demonstrate that the impact of

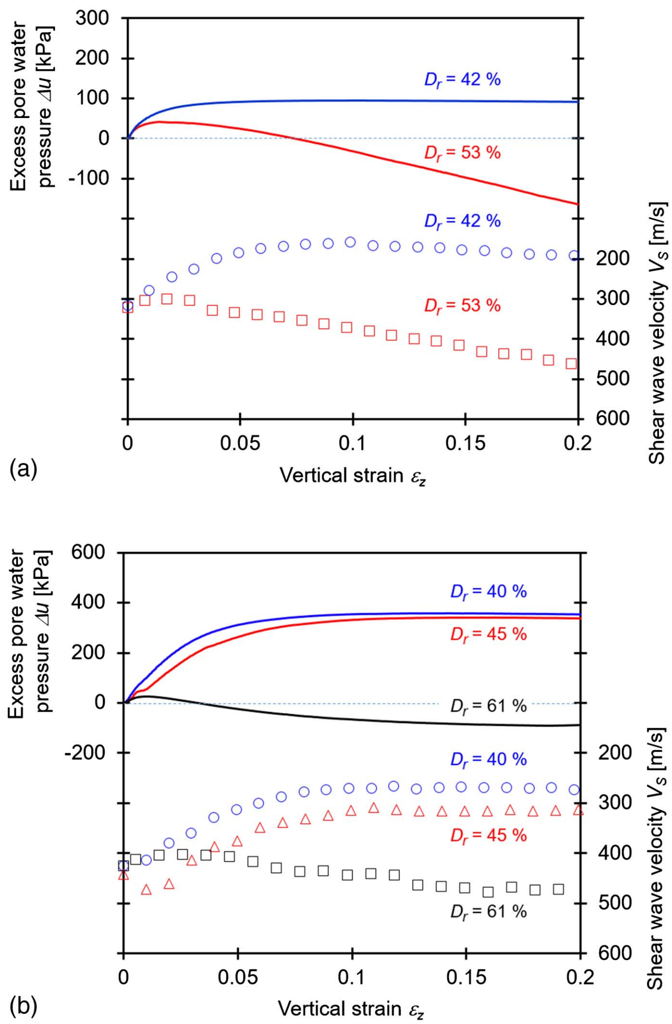

Fig. 4. Biopolymer-free sand: pore pressure and shear wave velocity response during undrained deviator loading. Initial isotropic effective confinement: (a) $\sigma_o' = 100$ kPa; and (b) $\sigma_o' = 400$ kPa.

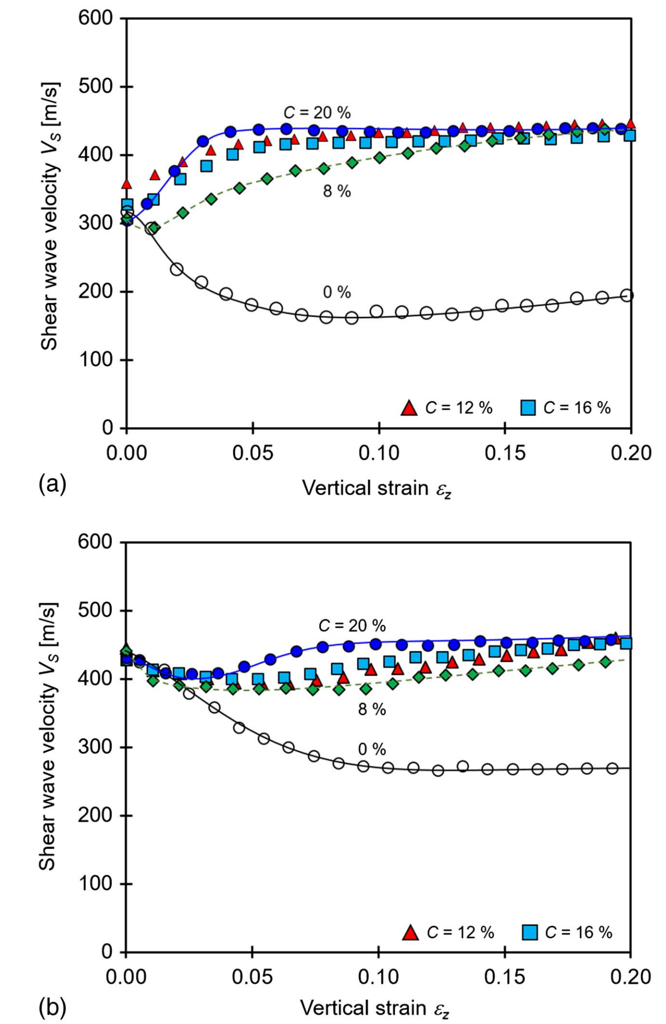

Fig. 5. Sand with CbG biopolymer and biopolymer-free sand. Evolution of shear wave velocity during undrained deviator loading. Initial isotropic effective stress: (a) $\sigma_o' = 100$ kPa; and (b) $\sigma_o' = 400$ kPa.

biopolymers on undrained shear strength is more pronounced at lower confining stress levels and for higher biopolymer concentrations. These observations are analogous to cementation treatments (Dupas and Pecker 1979; Acar and El-Tahir 1986; Dass et al. 1994; Fernandez and Santamarina 2001).

Role of Soft Viscoelastic Inclusion at the Particle Scale

Loose coarse-grained soils have a low coordination number and grains form granular columns that are prone to buckling due to the limited lateral support during loading, as depicted in Fig. 8(a) (Santamarina et al. 2001; Hasan et al. 2008; Kim et al. 2013; Kuei et al. 2020). Buckling collapse in loosely packed sands generates excess pore pressure under undrained conditions (Vaid and Chern 1985; Ishihara 1993).

Biopolymers such as gelatin fill the pore space, surround the particle chains, and contribute the viscoelastic resistance that prevents buckling. The spring-dashpot system in Fig. 8(b) is analogous to the pore-filling biopolymers (the elastic moduli and damping coefficients obtained for gelatin under longitudinal and shear vibrations are shown in Figs. S2 and S3). We anticipate that the grain support provided by the biopolymers differs with the loading rate due to their viscoelastic nature. Furthermore, the elastic modulus and viscous damping coefficient of gelatin are concentration dependent (Fig. S3); therefore, the increased gelatin concentration leads to greater lateral support to the granular frame and explains the increased undrained shear strength of the specimens that were consolidated before gelation [Fig. 7(a)].

Load–Deformation Response in p'-q-e Space

Effective stress and volumetric paths plotted in the p'-q-e space allow us to identify failure states and infer either contractive or dilative soil behavior. The hardened gelatin plugs pores and prevents pore pressure measurements. Yet, we can gain insight into the evolution of the mean effective stress $p' = (\sigma_1' + \sigma_3')/2$ from the measured shear wave velocity V_S (e.g., Knox et al. 1982; Cha et al. 2014)

$$V_S = \alpha\left(\frac{p'}{1\ \mathrm{kPa}}\right)^{\beta} \quad \text{thus} \quad \frac{p'}{1\ \mathrm{kPa}} = \left(\frac{V_S}{\alpha}\right)^{1/\beta} \tag{1}$$

where α = shear wave velocity at 1 kPa; and β = shear wave velocity sensitivity to changes in effective stress. Experimental results show $\alpha = 98.73$ m/s and $\beta = 0.25$ for the sand used in this study (Fig. S7).

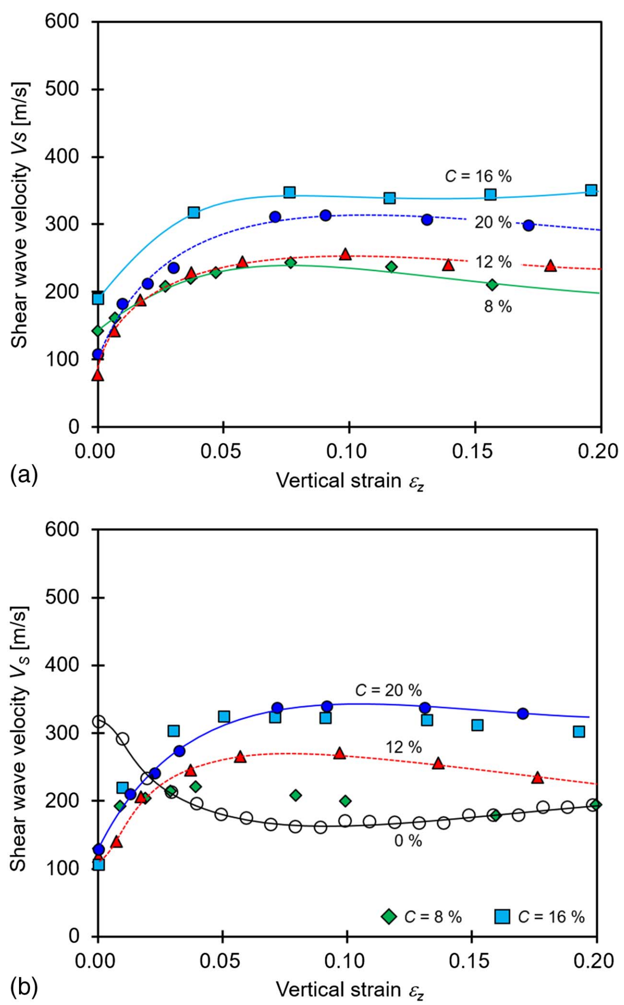

Fig. 6. Sand with CaG biopolymer. Evolution of shear wave velocity during undrained deviator loading. Initial isotropic confinement: (a) $\sigma_o = 50$ kPa; and (b) $\sigma_o = 100$ kPa.

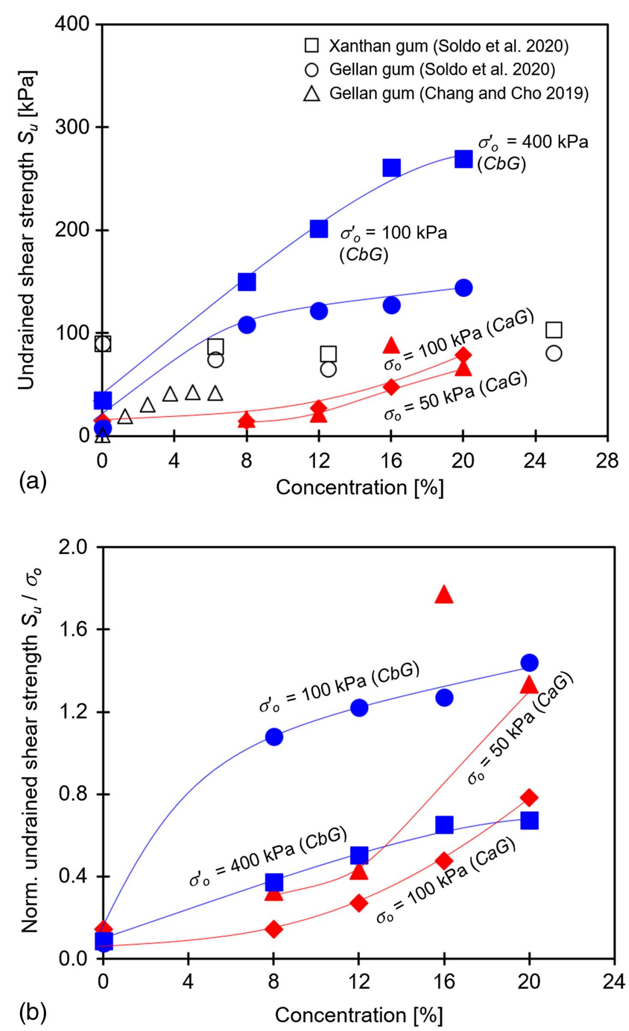

Fig. 7. Undrained shear strength S_u as a function of gelatin concentration and formation history: (a) data gathered in this study and published in the literature; and (b) undrained shear strength normalized by the initial confinement S_u/σ_o. Square and circle symbols: CbG specimens; triangle and diamond symbols: CaG specimens.

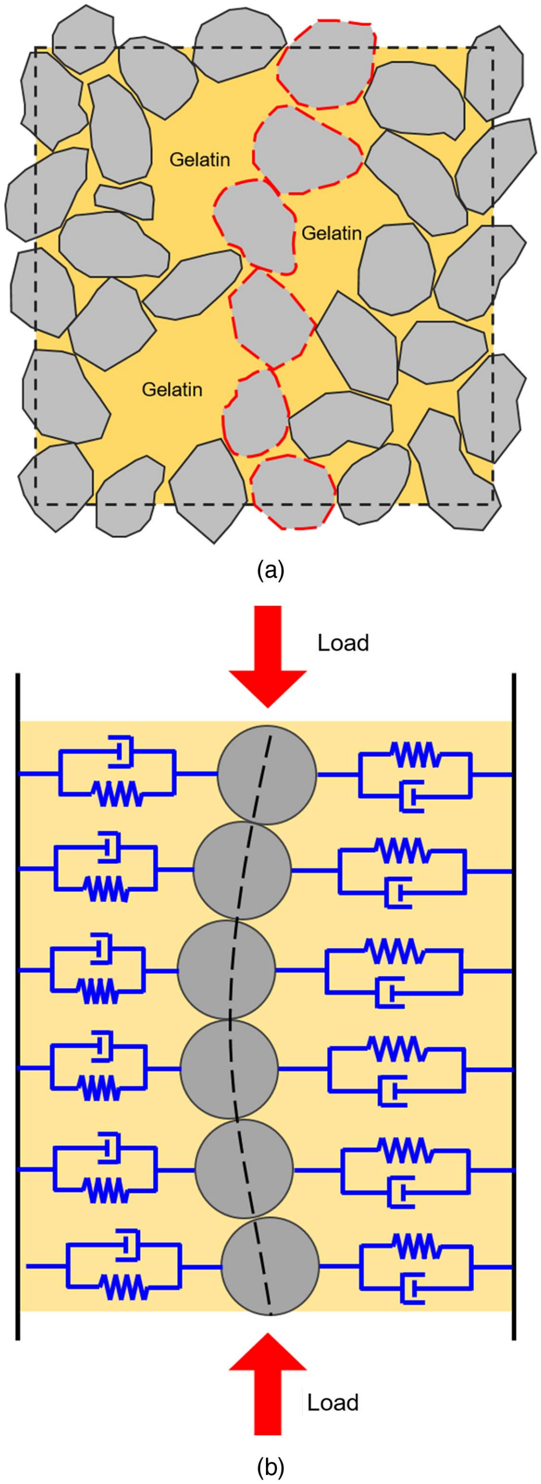

Fig. 8. Role of viscoelastic biopolymers on the response of contractive sands during undrained deviator loading: (a) loosely packed sand [poorly coordinated particle chains are prone to buckling (grains highlighted by long dashed lines)]; and (b) the viscoelastic forces exerted by the biopolymer hinders the buckling of particle chains.

Figs. 9 and 10 show the effective stress paths inferred from changes in the shear wave velocity for CbG and CaG specimens. These figures also include the paths measured for the biopolymer-free specimens during undrained loading. The baseline cases show the consequences of the excess pore pressure generation during undrained shearing in both contractive specimens (positive excess pressure and postpeak softening behavior) as well as dilative specimens (negative excess pore pressure). The biopolymer-treated loose specimens show increases in effective stress p' due to the presence of biopolymers together with a strain-hardening behavior that is compatible with a dilative tendency (Fig. 9). Terminal states appear to be affected by gelatin concentration.

The estimated initial mean effective stress p' is significantly lower than the applied confining stress σ_o in CaG specimens (Fig. 10). Still, the presence of gelatin hinders bucking and particle rearrangement, which results in the high peak deviator stress $q_{\max}$ of treated sands. Furthermore, postpeak softening decreases with higher gelatin concentrations, suggesting that gelatin tears at large strains.

Loading-Gelation History and Implications on Field Implementation

CbG cases simulate the condition where a contractive soil layer prone to liquefaction is treated by injecting a viscoelastic biopolymer grout, whereas CaG resembles cases where the viscoelastic grout treatment is applied at every lift during backfilling.

Results in Figs. 9 and 10 show that the confinement-gelation sequence has a pronounced effect on the undrained shear strength. The marked improvement in undrained shear strength in CbG specimens compared to the CaG specimens has important implications on field implementation of biopolymer grout injections. In particular, this finding highlights potential benefits of treating the soil postconstruction rather than before or during construction.

Still, the field implementation of biopolymer treatments in geotechnical practice faces a number of uncertainties related to the durability and life span associated with thermal and moisture cycles, indigenous microbial activity, pore water chemistry, and groundwater flow–driven dissolution.

Conclusions

This study investigated the undrained load–deformation behavior of biopolymer-treated contractive sands by conducting triaxial compression tests while monitoring the shear wave velocity. Our results reveal that the presence of gel-type biopolymers in pores has pronounced effects on sand behavior. Salient findings from this experimental study are as follows:

- Viscoelastic pore fillers hinder granular chain buckling and particle rearrangement. Therefore, biopolymers alter the contractive behavior and postpeak softening of loose sands during undrained shear. This effect becomes more pronounced as the biopolymer concentration and stiffness increases.
- The shear wave velocity can be used to infer changes in the effective stress carried by the granular structure. The shear wave velocity of biopolymer-treated sands increases during undrained deviator loading, which indicates the increase in the mean effective stress felt by the granular structure. The inferred effective stress paths exhibit a dilative-type strain-hardening response for the biopolymer-treated loose sands.
- Viscoelastic pore fillers alter the terminal state in the p'-q-e space. Therefore, critical states should be reconsidered for biopolymer-treated sands.
- The confinement-gelation sequence has a pronounced effect on the undrained shear strength. The gelated biopolymer does not drain during confinement (CaG sequence). Consequently, CbG leads to greater undrained shear strength.
- The field implementation of biopolymer treatments must consider the load-gelation history, gel concentration, and confining stress.

J. Geotech. Geoenviron. Eng., 2021, 147(8): 04021072

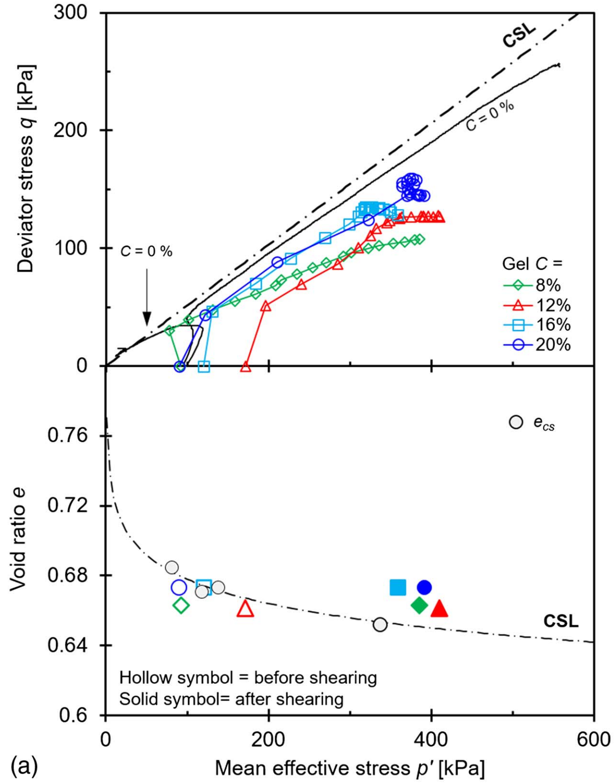

Fig. 9. Shear response in p'-q-e space: CbG. Initial isotropic stress: (a) $\sigma_o' = 100$ kPa; and (b) $\sigma_o' = 400$ kPa. The critical state line (CSL) is taken from Park and Santamarina (2020): $\alpha = 27.3°\,(\phi_{cs} = 31°)$; $\eta_{cs} = 0.52$.

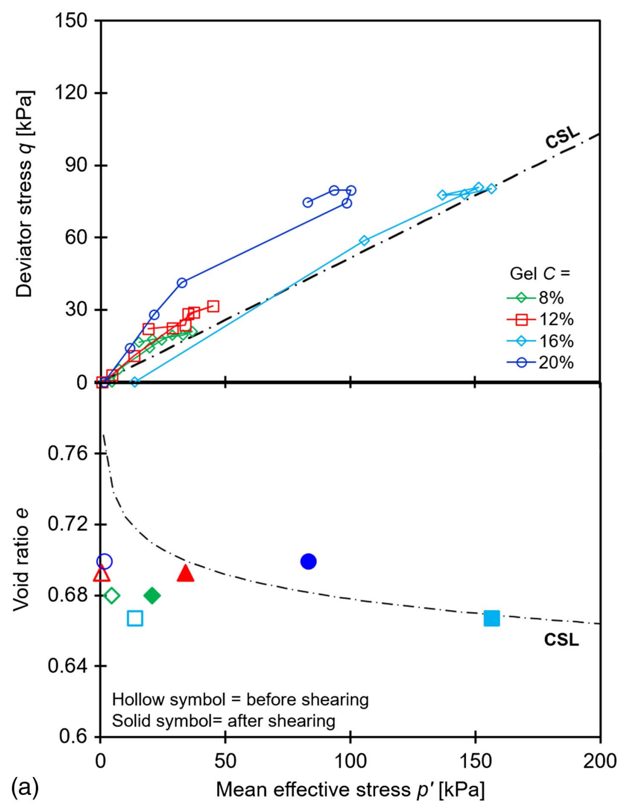

Fig. 10. Shear response in p'-q-e space: CaG. Initial isotropic stress: (a) $\sigma_o = 50$ kPa; and (b) $\sigma_o = 100$ kPa. The critical state line (CSL) is taken from Park and Santamarina (2020): $\alpha = 27.3°\,(\phi_{cs} = 31°)$; $\eta_{cs} = 0.52$.

Data Availability Statement

All data, models, and code used to support the findings of this study are available from the corresponding author upon request.

Acknowledgments

We would like to thank two anonymous reviewers, the associate editor, and the editor Dr. John McCartney for providing valuable comments and suggestions. This research was supported by the National Research Foundation of Korea (NRF) grant funded by the Korean government (Ministry of Science, ICT and Future Planning) (No. 2020R1A2C4002358), a grant (19CTAP-C151917-01) from the Technology Advancement Research Program (TARP) funded by the Ministry of Land, Infrastructure, and Transport of the Korean government, and the KAUST Endowment. Gabrielle E. Abelskamp edited this manuscript.

Supplemental Materials

Figs. S1–S7 and Table S1 are available online in the ASCE Library (www.ascelibrary.org).

References

Acar, Y. B., and E.-T. A. El-Tahir. 1986. "Low strain dynamic properties of artificially cemented sand." *J. Geotech. Eng.* 112 (11): 1001–1015. https://doi.org/10.1061/(ASCE)0733-9410(1986)112:11(1001).

Airey, D. W., and M. Fahey. 1991. "Cyclic response of calcareous soil from the North-West Shelf of Australia." *Géotechnique* 41 (1): 101–121. https://doi.org/10.1680/geot.1991.41.1.101.

Aloufi, M., and J. C. Santamarina. 1995. "Low and high-strain macrobehavior of grain masses: The effect of particle eccentricity." *Trans. ASAE* 38 (3): 877–887. https://doi.org/10.13031/2013.27904.

ASTM. 2011. *Standard test method for consolidated undrained triaxial compression test for cohesive soils*. ASTM D4767. West Conshohocken, PA: ASTM.

Bogue, R. H. 1923. "Conditions affecting the hydrolysis of collagen to gelatin." *Ind. Eng. Chem.* 15 (11): 1154–1159. https://doi.org/10.1021/ie50167a018.

Bohidar, H. B., and S. S. Jena. 1993. "Kinetics of sol–gel transition in thermoreversible gelation of gelatin." *J. Chem. Phys.* 98 (11): 8970–8977. https://doi.org/10.1063/1.464456.

Cabalar, A. F., M. Wiszniewski, and Z. Skutnik. 2017. "Effects of xanthan gum biopolymer on the permeability, odometer, unconfined compressive and triaxial shear behavior of a sand." *Soil Mech. Found. Eng.* 54 (5): 356–361. https://doi.org/10.1007/s11204-017-9481-1.

Casagrande, A. 1976. *Liquefaction and cyclic deformation of sands, a critical review.* Cambridge, MA: Harvard University Press.

Castro, G. 1969. *Liquefaction of sands*. Cambridge, MA: Harvard University Press.

Cha, M., J. C. Santamarina, H.-S. Kim, and G.-C. Cho. 2014. "Small-strain stiffness, shear-wave velocity, and soil compressibility." *J. Geotech. Geoenviron. Eng.* 140 (10): 06014011. https://doi.org/10.1061/(ASCE)GT.1943-5606.0001157.

Chang, I., and G. C. Cho. 2012. "Strengthening of Korean residual soil with β-1, 3/1, 6-glucan biopolymer." *Constr. Build. Mater.* 30 (May): 30–35. https://doi.org/10.1016/j.conbuildmat.2011.11.030.

Chang, I., and G. C. Cho. 2019. "Shear strength behavior and parameters of microbial gellan gum-treated soils: From sand to clay." *Acta Geotech.* 14 (2): 361–375. https://doi.org/10.1007/s11440-018-0641-x.

Chen, R., L. Zhang, and M. Budhu. 2013. "Biopolymer stabilization of mine tailings." *J. Geotech. Geoenviron. Eng.* 139 (10): 1802–1807. https://doi.org/10.1061/(ASCE)GT.1943-5606.0000902.

Cho, G. C., and I. Chang. 2018. "Cementless soil stabilizer—Biopolymer." In *Proc., 2018 World Congress on Advances in Civil, Environmental, & Materials Research*. Daejeon, Korea: International Association of Structural Engineering and Mechanics.

Clough, G. W., N. Sitar, R. C. Bachus, and N. S. Rad. 1981. "Cemented sands under static loading." *J. Geotech. Eng. Div.* 107 (6): 799–817. https://doi.org/10.1061/AJGEB6.0001152.

Consoli, N. C., R. C. Cruz, M. F. Floss, and L. Festugato. 2010. "Parameters controlling tensile and compressive strength of artificially cemented sand." *J. Geotech. Geoenviron. Eng.* 136 (5): 759–763. https://doi.org/10.1061/(ASCE)GT.1943-5606.0000278.

Dai, S., and J. C. Santamarina. 2017. "Stiffness evolution in frozen sands subjected to stress changes." *J. Geotech. Geoenviron. Eng.* 143 (9): 04017042. https://doi.org/10.1061/(ASCE)GT.1943-5606.0001713.

Dass, R. N., S. C. Yen, B. M. Das, V. K. Puri, and M. A. Wright. 1994. "Tensile stress-strain characteristics of lightly cemented sand." *Geotech. Test. J.* 17 (3): 305–314. https://doi.org/10.1520/GTJ10105J.

DeJong, J. T., B. M. Mortensen, B. C. Martinez, and D. C. Nelson. 2010. "Bio-mediated soil improvement." *Ecol. Eng.* 36 (2): 197–210. https://doi.org/10.1016/j.ecoleng.2008.12.029.

Dupas, J.-M., and A. Pecker. 1979. "Static and dynamic properties of sand-cement." *J. Geotech. Eng. Div.* 105 (3): 419–436. https://doi.org/10.1061/AJGEB6.0000778.

Fam, M., and J. C. Santamarina. 1995. "Study of geoprocesses with complementary mechanical and electromagnetic wave measurements in an oedometer." *Geotech. Test. J.* 18 (3): 307–314. https://doi.org/10.1520/GTJ10999J.

Fernandez, A. L., and J. C. Santamarina. 2001. "Effect of cementation on the small-strain parameters of sands." *Can. Geotech. J.* 38 (1): 191–199. https://doi.org/10.1139/t00-081.

Gallagher, P. M., and J. K. Mitchell. 2002. "Influence of colloidal silica grout on liquefaction potential and cyclic undrained behavior of loose sand." *Soil Dyn. Earthquake Eng.* 22 (9–12): 1017–1026. https://doi.org/10.1016/S0267-7261(02)00126-4.

Gómez-Estaca, J., M. C. Gómez-Guillén, F. Fernández-Martín, and P. Montero. 2011. "Effects of gelatin origin, bovine-hide and tuna-skin, on the properties of compound gelatin–chitosan films." *Food Hydrocolloids* 25 (6): 1461–1469. https://doi.org/10.1016/j.foodhyd.2011.01.007.

Ham, S.-M., I. Chang, D.-H. Noh, T.-H. Kwon, and B. Muhunthan. 2018. "Improvement of surface erosion resistance of sand by microbial biopolymer formation." *J. Geotech. Geoenviron. Eng.* 144 (7): 06018004. https://doi.org/10.1061/(ASCE)GT.1943-5606.0001900.

Hardin, B. O., and V. P. Drnevich. 1972. "Shear modulus and damping in soils: Measurement and parameter effects." *J. Soil Mech. Found. Div.* 98 (6): 603–624. https://doi.org/10.1061/JSFEAQ.0001756.

Hasan, A., K. Alshibli, H. Jaeger, and M. Rivers. 2008. "Visualization of shear band in sand using synchrotron micro-tomography." In *Geo-Congress 2008: Characterization, Monitoring, and Modeling of GeoSystems, Geotechnical Special Publication 179*, edited by A. N. Alshawabkeh, K. R. Reddy, and M. V. Khire. Reston, VA: ASCE. https://doi.org/10.1061/40972(311)129.

Im, J., A. T. Tran, I. Chang, and G. C. Cho. 2017. "Dynamic properties of gel-type biopolymer-treated sands evaluated by resonant column (RC) tests." *Geomech. Eng.* 12 (5): 815–830. https://doi.org/10.12989/gae.2017.12.5.815.

Imeson, A. 2010. *Food stabilizers, thickeners and gelling agents*. Chichester, UK: Wiley-Blackwell.

Ishihara, K. 1993. "Liquefaction and flow failure during earthquakes." *Géotechnique* 43 (3): 351–451. https://doi.org/10.1680/geot.1993.43.3.351.

Ivanov, V., and J. Chu. 2008. "Applications of microorganisms to geotechnical engineering for bioclogging and biocementation of soil in situ." *Rev. Environ. Sci. Biotechnol.* 7 (2): 139–153. https://doi.org/10.1007/s11157-007-9126-3.

Karol, R. H. 2003. *Chemical grouting and soil stabilization*. 3rd ed. Boca Raton, FL: CRC Press.

Kavanagh, J. L., T. Menand, and K. A. Daniels. 2013. "Gelatine as a crustal analogue: Determining elastic properties for modelling magmatic intrusions." *Tectonophysics* 582 (Jan): 101–111. https://doi.org/10.1016/j.tecto.2012.09.032.

Khan, Z. I., A. Hussain, M. Ashraf, and L. R. McDowell. 2006. "Mineral status of soils and forages in Southwestern Punjab-Pakistan:

Micro-minerals." *Asian-Aust. J. Anim Sci.* 19 (8): 1139–1147. https://doi.org/10.5713/ajas.2006.1139.

Kim, F. H., D. Penumadu, J. Gregor, N. Kardjilov, and I. Manke. 2013. "High-resolution neutron and X-ray imaging of granular materials." *J. Geotech. Geoenviron.* 139 (5): 715–723. https://doi.org/10.1061/(ASCE)GT.1943-5606.0000809.

Kim, Y. M., T. Park, and T. H. Kwon. 2019. "Engineered bioclogging in coarse sands by using fermentation-based bacterial biopolymer formation." *Geomech. Eng.* 17 (5): 485–496. https://doi.org/10.12989/gae.2019.17.5.485.

Knox, D. P., K. H. Stokoe, and S. E. Kopperman. 1982. *Effect of state of stress on velocity of low-amplitude shear waves propagating along principal stress directions in dry sand*. Technical Rep. GR 82-23. Austin, TX: Univ. of Texas at Austin.

Kuei, K. C., J. T. DeJong, and A. Martinez. 2020. "Particle size effects on the strength and fabric of granular media." In *Geo-Congress 2020: Modeling, Geomaterials, and Site Characterization, Geotechnical Special Publication 317*, edited by J. P. Hambleton, R. Makhnenko, and A. S. Budge. Reston, VA: ASCE. https://doi.org/10.1061/9780784482803.038.

Kwon, T. H., D. H. Noh, S. M. Ham, Y. M. Kim, and M. K. Jeon. 2017. "Impact of bacterial biopolymer formation on hydraulic conductivity, erosion resistance and seismic response of sands." In *Proc., 19th Int. Conf. on Soil Mechanics and Geotechnical Engineering (ICSMGE)*. London: International Society for Soil Mechanics and Geotechnical Engineering.

Kwon, Y. M., S. M. Ham, T. H. Kwon, G. C. Cho, and I. Chang. 2019. "Surface-erosion behaviour of biopolymer-treated soils assessed by EFA." *Geotech. Lett.* 10 (2): 106–112. https://doi.org/10.1680/jgele.19.00106.

Lade, P. V., and D. D. Overton. 1989. "Cementation effects in frictional materials." *J. Geotech. Eng.* 115 (10): 1373–1387. https://doi.org/10.1061/(ASCE)0733-9410(1989)115:10(1373).

Latifi, N., S. Horpibulsuk, C. L. Meehan, M. Z. Abd Majid, M. M. Tahir, and E. T. Mohamad. 2016. "Improvement of problematic soils with biopolymer—An environmentally friendly soil stabilizer." *J. Mater. Civ. Eng.* 29 (2): 04016204. https://doi.org/10.1061/(ASCE)MT.1943-5533.0001706.

Muguda, S., S. J. Booth, P. N. Hughes, C. E. Augarde, C. Perlot, A. W. Bruno, and D. Gallipoli. 2017. "Mechanical properties of biopolymer-stabilised soil-based construction materials." *Geotech. Lett.* 7 (4): 309–314. https://doi.org/10.1680/jgele.17.00081.

Park, J., and J. C. Santamarina. 2020. "Soil response to repetitive changes in pore-water pressure under deviatoric loading." *J. Geotech. Geoenviron.* 146 (5): 04020023. https://doi.org/10.1061/(ASCE)GT.1943-5606.0002229.

Robertson, P. K., and C. E. Wride. 1998. "Evaluating cyclic liquefaction potential using the cone penetration test." *Can. Geotech. J.* 35 (3): 442–459. https://doi.org/10.1139/t98-017.

Santamarina, J. C., A. Klein, and M. A. Fam. 2001. *Soils and waves*. New York: Wiley.

Santamarina, J. C., L. A. Torres-Cruz, and R. Bachus. 2019. "Why coal ash and tailings dam disasters occur: Knowledge gaps and management shortcomings contribute to catastrophic dam failures." *Science* 364 (6440): 526–528. https://doi.org/10.1126/science.aax1927.

Schofield, A., and P. Wroth. 1968. *Critical state soil mechanics*. London: McGraw-Hill.

Soldo, A., M. Miletić, and M. L. Auad. 2020. "Biopolymers as a sustainable solution for the enhancement of soil mechanical properties" *Sci. Rep.* 10 (1): 1–13. https://doi.org/10.1038/s41598-019-57135-x.

Terzaghi, K., R. B. Peck, and G. Mesri. 1967. *Soil mechanics in engineering practice*. New York: Wiley.

Thevanayagam, S. 1998. "Effect of fines and confining stress on undrained shear strength of silty sands." *J. Geotech. Geoenviron. Eng.* 124 (6): 479–491. https://doi.org/10.1061/(ASCE)1090-0241(1998)124:6(479).

Tran, A. T. P., I. Chang, and G. C. Cho. 2019. "Soil water retention and vegetation survivability improvement using microbial biopolymers in drylands." *Geomech. Eng.* 17 (5): 475–483. https://dx.doi.org/10.12989/gae.2019.17.5.475.

Vaid, Y. P., and J. C. Chern. 1985. "Cyclic and monotonic undrained response of sands." In *Proc., Advances in the Art of Testing Soils under Cyclic Loading Conditions*, edited by V. Khosla, 120–147. Reston, VA: ASCE.

Wang, Y. H., and S. C. Leung. 2008. "Characterization of cemented sand by experimental and numerical investigations." *J. Geotech. Geoenviron. Eng.* 134 (7): 992–1004. https://doi.org/10.1061/(ASCE)1090-0241(2008)134:7(992).

Wood, D. M. 1990. *Soil behaviour and critical state soil mechanics*. Cambridge, UK: Cambridge University Press.

Xanthakos, P. P. 1994. *Slurry walls as structural systems*. New York: McGraw-Hill.

Yamamuro, J. A., and P. V. Lade. 1997. "Static liquefaction of very loose sands." *Can. Geotech. J.* 34 (6): 905–917. https://doi.org/10.1139/t97-057.

Yoshimine, M., P. K. Robertson, and C. E. Wride. 1999. "Undrained shear strength of clean sands to trigger flow liquefaction." *Can. Geotech. J.* 36 (5): 891–906. https://doi.org/10.1139/t99-047.

Yun, T. S., and J. C. Santamarina. 2005. "Decementation, softening, and collapse: Changes in small-strain shear stiffness in k_0 loading." *J. Geotech. Geoenviron. Eng.* 131 (3): 350–358. https://doi.org/10.1061/(ASCE)1090-0241(2005)131:3(350).